Chemical Geology 506 (2019) 68–78

Contents lists available at ScienceDirect

Chemical Geology

journal homepage: www.elsevier.com/locate/chemgeo

Tracing the palaeoredox conditions at Forsmark, Sweden, using uranium mineral geochronology

Lindsay Krall[a,b,*], Lena Z. Evins[b], Ellen Kooijman[c], Martin Whitehouse[c], Eva-Lena Tullborg[d]

[a] The George Washington University, 2121 Eye Street NW, Washington, DC 20052, USA
[b] The Swedish Nuclear Fuel and Waste Management Company (SKB), Evenemangsgatan 13, SE-169 03 Solna, Sweden
[c] Department of Geosciences, Swedish Museum of Natural History, Box 50 007, 104 05 Stockholm, Sweden
[d] Terralogica AB, Gråbo. Östra Annekärrsvägen 17, SE-443 72 Gråbo, Sweden

ARTICLE INFO

Editor: Michael E. Böttcher

Keywords:
Geochronology
Uranyl silicates
Uraninite
Deep groundwater
Water-rock interaction
Hydrothermal fluids
Oxidation

ABSTRACT

U-Pb isotope systems have been used to constrain the timing of formation, alteration, and oxidation of U minerals from the meta-granitic bedrock at Forsmark, eastern Sweden. Secondary ion mass spectrometry (SIMS) has been used to collect U-Pb data from uraninite. Discordant data suggest a ~1.8 Ga emplacement of uraninite-bearing pegmatites and an event of uraninite alteration at ~1.6 Ga. The latter age is contemporaneous with the Gothian orogeny in Scandinavia, which was associated with hydrothermal fluid circulation in the Fennoscandian Shield. Ca-uranyl silicates haiweeite and uranophane predominately formed 1.3–1.2 Ga, contemporaneous with the emplacement of the Satakunta complex of the Central Scandinavian Dolerite Group. A Palaeozoic group of Ca-U(VI)-silicates is also present, which indicates that the geochemical composition of geologic fluids was heterogeneous throughout the fracture network during this time. Low Pb concentrations in the U(VI) silicates of several samples are compatible with a recent (< 100 Ma) alteration or precipitation of these minerals in connection to reaction with carbonate-rich fluids. The results support a geologically early oxidation of U(IV) to U(VI) and provide insight into the palaeoredox conditions that may impart an on-going influence on the mobility of natural U in the Forsmark fracture network.

1. Introduction

Forsmark, Sweden, has been proposed by the Swedish Nuclear Fuel and Waste Management Company to host a deep, geological repository for spent nuclear fuel (SNF) and presently hosts a repository for low- and intermediate-level radioactive waste (SFR). Since SNF is predominantly UO_2, it is important to understand the geochemistry and mobility of uranium in the repository environment and surrounding bedrock (SKB, 2008). During the Forsmark site investigations (2002–2008), several groundwater samples from intermediate depth (400–700 m below sea level; hereafter "m.b.s.l.") were found to contain dissolved natural uranium in concentrations elevated with respect to groundwater origin and redox potential (Smellie et al., 2008).

Preliminary geochemical modelling indicated that if a solid U(VI)-phase is in contact with groundwaters, aqueous U(VI)-carbonate complexes can retain U(VI) in solution even at Eh −200 to −140 mV (Smellie et al., 2008). Through characterization of the U(IV) and U(VI) minerals in Forsmark pegmatites and fracture fillings, Krall et al. (2015) postulated that local U(IV) was initially oxidized during early events of hydrothermal fluid circulation as presented by Sandström et al. (2009). Nevertheless, the chemical results could not preclude a relation between U oxidation and episodic deglaciation, which may occur within the future timeframe of the SNF fuel repository safety case (Näslund et al., 2013). Therefore, it is of interest to determine the timing of U mineral formation and alteration in order to understand the response of the U redox system to geologic fluid circulation over time.

The present study aims to develop a geochronological framework for the geochemical events recorded by the uranium minerals in the Forsmark bedrock. This is accomplished through Secondary Ion Mass Spectrometry (SIMS) and laser ablation-inductively coupled plasma-mass spectrometry (LA-ICP-MS) U-Pb analyses of U(IV)-bearing uraninite and the U(VI) minerals haiweeite and uranophane at Forsmark. Constraints on the timing of U(VI) mineral formation will provide insight into the timing and geochemical conditions of the initial oxidation of U(IV) to U(VI) at Forsmark.

* Corresponding author.
E-mail address: lkrall@email.gwu.edu (L. Krall).

https://doi.org/10.1016/j.chemgeo.2018.12.013
Received 12 February 2018; Received in revised form 13 December 2018; Accepted 17 December 2018
Available online 30 December 2018

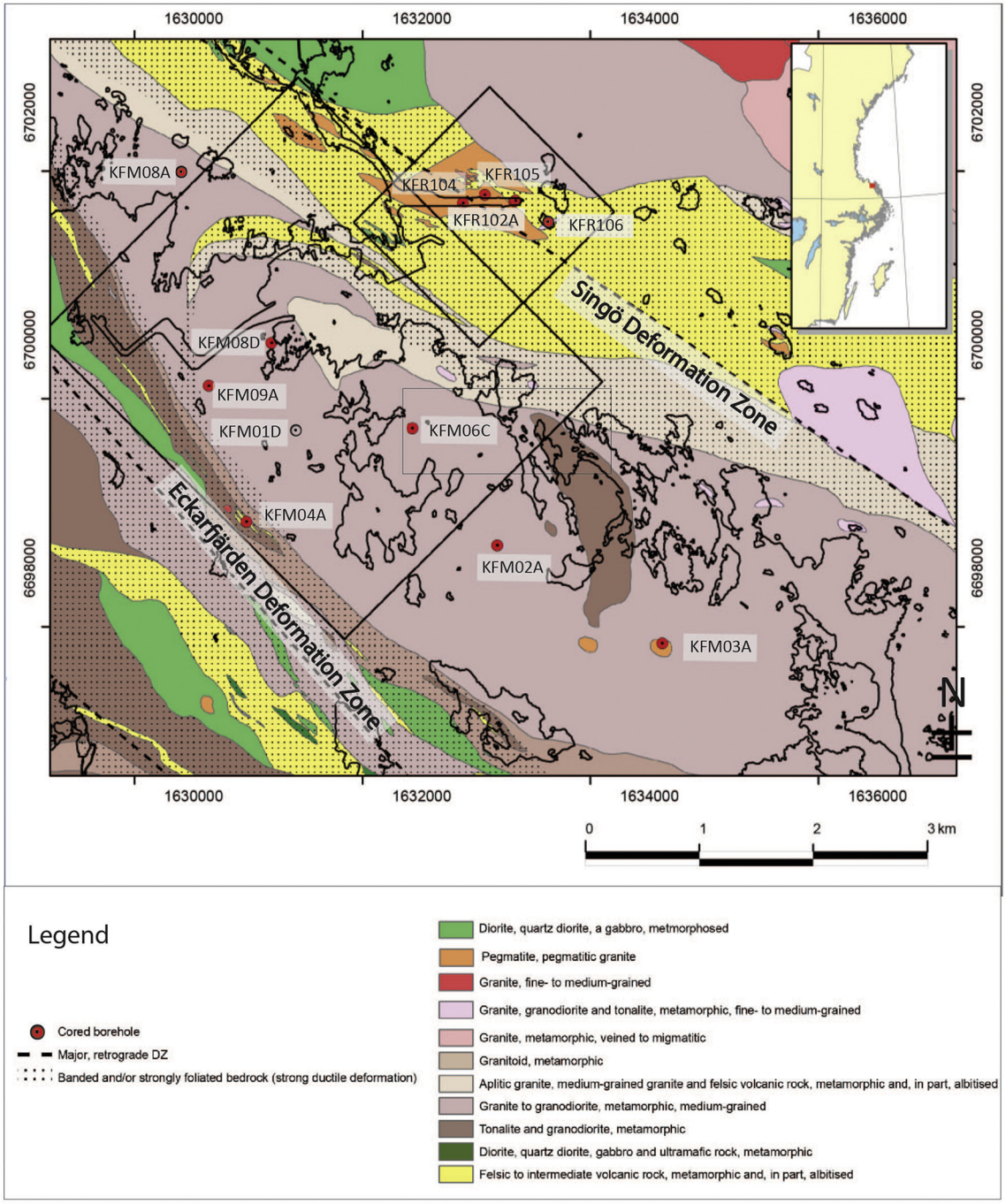

Fig. 1. Bedrock geological map of Forsmark (Sweden top right corner) showing boreholes in which uranium mineral chemistry reported by Krall et al. (2015) and Sandström et al. (2011). Current isotopic data reported from KFM01D, KFM04A, KFR106, KFM02A, and KFR102A.

2. Background

2.1. Geological setting and history

Forsmark, located approximately 120 km north of Stockholm in eastern Sweden, is situated within the Svecokarelian orogeny in the southwestern region of the Fennoscandian Shield (Fig. 1). This region is dominated by intrusive rocks and felsic volcanic rocks, the majority of which have been affected by strong ductile deformation under amphibolite-facies metamorphism. Crystallization and ductile deformation of the igneous rocks occurred between 1.9 and 1.8 Ga (Stephens and Andersson, 2015). The volume at Forsmark targeted to host the SNF repository is situated within a tectonic lens. This lens has been affected by ductile strain to a lesser degree than the belts of high ductile strain by which it is bound.

Sometime between 1.8 and 1.7 Ga, the deformation shifted from ductile to brittle (Söderlund et al., 2008). After 1.8 Ga, the Forsmark fracture network may have been influenced by intrusion of the Transscandinativian Igneous Belt at 1.8–1.7 Ga (e.g. Larson and Berglund, 1992; Åhäll and Larson, 2000; Gorbatschev, 2004); and by far-field effects of the Gothian orogeny at 1.7–1.5 Ga (e.g. Connelly and Åhäll, 1996; Åhäll and Gower, 1997), the intrusion of Rapakivi granites between 1.67 and 1.47 Ga (Haapala et al., 2005), the Hallandian orogeny at 1.5–1.4 Ga (e.g. Hubbard, 1975; Christoffel et al., 1999; Möller et al., 2007), intrusion of the Central Scandinavian Dolerite Group between 1.25 and 1.27 Ga (Söderlund et al., 2005, 2006; Hogmalm et al., 2006),

and possible far-field effects of the Sveconorwegian orogeny at 1.1–0.9 Ga (Bingen et al., 2008), and the Caledonian orogeny at 510–400 Ma (Gee and Sturt, 1985; Roberts, 2003). During the Phanerozoic, the Forsmark area was also influenced by rifting during the Late Carboniferous to Permian and Mesozoic, crustal shortening during the Late Cretaceous and Palaeogene (Laramide/Alpine), and ridge push from the mid-Atlantic ridge during the Neogene and Quaternary (Saintot et al., 2011, and references therein).

Sandström et al. (2008, 2009) identified and characterized four generations of fracture minerals to constrain the brittle deformational history of the Forsmark site. On the basis of ^{40}Ar-^{39}Ar geochronology, two periods of hydrothermal fluid circulation were suggested to have occurred as far-field effects of tectonic events in Scandinavia (Sandström et al., 2009). Both events are manifest by hematite-staining of the bedrock through oxidation of Fe(II). The oldest generation of fracture minerals includes epidote, quartz, and chlorite. These formed between 1.8 and 1.1 Ga, during either the Svecokarelian orogeny at 1.8–1.7 Ga when brittle conditions began to prevail (200–300 °C) or the Gothian orogeny at 1.6–1.5 Ga, the latter of which is consistent with geochronological analyses of fractures south of Forsmark (Wickman et al., 1983). The second event of hydrothermal fluid circulation (150–250 °C) led to the formation of adularia, albite, calcite, prehnite, laumontite, and chlorite/corrensite. Through ^{40}Ar-^{39}Ar geochronology, this event was constrained to 1.1–1.0 Ga and was therein inferred to have been activated by the Sveconorwegian orogeny (Sandström et al., 2009).

During the Palaeozoic, fluids migrated downward from an organic-rich sedimentary overburden within the sub-Cambrian peneplain, which covered the Palaeoproterozoic crystalline rocks in the Forsmark area (Cederbom et al., 2000). These fluids mixed with basinal brines to form sulfide minerals, including pyrite and galena, in addition to quartz, calcite, corrensite, analcime, and adularia. This third event of fluid circulation was constrained to 456–277 Ma through ^{40}Ar-^{39}Ar geochronology of adularia (Sandström et al., 2009). The fourth generation, formed in the time interval 277 m.y. to the present, is characterized by precipitation of clay minerals, calcite, goethite, and pyrite. Several cycles of glacial loading and unloading have occurred during the Quaternary. More recently, (de)glaciation events of the Holocene have disturbed the hydrogeochemistry through intrusion of glacial meltwaters and of Littorina Seawater (a 9.0–5.0 ka predecessor to the modern Baltic Sea; Laaksoharju et al., 2008).

2.2. Regional and local U minerals

Welin (1963, 1964, 1966a, 1992) investigated the U-Pb systems of uranium minerals collected from the tailing piles of Swedish iron mines, including four in the Forsmark region, to contextualize the deposition of uranium within the geological history of Scandinavia. The oldest mineralization, of subhedral uraninite within amphibolite skarn, was dated to 1.760 Ga which coincided with the formation of the late kinematic granites and pegmatites in Central Sweden (Welin, 1963, 1980). Additionally, secondary botryoidal uraninite was deposited within veins of calcite, chlorite, and hematite (Welin, 1963). This was originally determined to occur at 1.585 Ga (Welin, 1963) but we have recalculated the date to 1.565 Ga using the ratios reported by Welin (1963) together with modern decay constants. Thus, the deposition is connected to the Gothian orogeny (Welin, 1963) or the intrusion of the Åland rapakivi massif at ~1.57 Ga (Welin, 1992; Heinonen et al., 2010). Analyses from both the subhedral and botryoidal uraninite show a Pb-loss event at ~300 Ma (Welin, 1963).

Krall et al. (2015) characterized uranium minerals from Forsmark drillcores by using an electron probe mircoanalyzer (EPMA) and petrographic microscopy. Primary uraninite and amorphous uranothorite in several pegmatites were interpreted to have been altered by hydrothermal fluids on the basis of enrichment in Ca, Si, and Al. Primary pegmatitic uraninite was dated to 2.2–1.8 Ga following the chemical dating method of Bowles (1990). Ca-U(VI)-silicates haiweeite and uranophane are associated with primary uraninite and uranothorite and with chlorite, calcite, and reddish Fe-(oxyhydr)oxides in veins in the pegmatites. On the basis of chemical composition and textural relations, haiweeite was interpreted to have formed during the early circulation of hydrothermal fluids. Additionally, < 10 μm precipitates of variably Si-enriched U(VI)/U(IV)-(hydr)oxides are associated with Fe-Al-silicates, particularly chlorite. On the basis of elevated phosphorous and yttrium concentrations (up to 2.2 and 17.5 wt% P_2O_5 and Y_2O_3, respectively), these phases were suggested by Krall et al. to have formed during the Palaeozoic. In several samples, uranophane, the most abundant U(VI) mineral, and haiweeite, appeared to have been partially dissolved by carbonate-rich fluids, based on the textural relation with calcite. Since calcite is prevalent in each of the second, third, and fourth generations of fracture minerals, the timing of U(VI)-silicate alteration could not be constrained (Krall et al., 2015).

2.3. U migration and glacial cycles in crystalline rock

The impact of episodic glaciation on the groundwater geochemistry warrants consideration in a safety analysis for a deep-mined repository in continental shield rocks, such as the Fennoscandian and the Canadian Shields. Therefore, the Palmottu Natural Analogue Project (Finland) aimed to address the migration of U in crystalline bedrock, and the Greenland Analogue Project targeted the impact of a glaciation on the subsurface environment in crystalline bedrock. Uranium-series disequilibrium analyses of samples from as deep as 100 m.b.s.l. at Palmottu showed periodic accumulation of uranium on fracture surfaces at 40, 60, and 110 ka, potentially in connection to glacial events. However, mobilization of U was not observed at depths > 80 m.b.s.l (Suksi et al., 2001). The Greenland Analogue Project showed that glacial meltwater can penetrate to depths of 500 m.b.s.l., and that oxidation of pyrite and formation of FeOOH is common down to 50 m.b.s.l. but in more conductive zones may occur as deep as 250 m.b.s.l. (Drake et al., 2017a).

Uranium-series disequilibrium analyses of fracture surfaces from the Forsmark site showed redistribution of uranium at depths > 300 m.b.s.l. within the last 1 Ma (Tullborg et al., 2017). This finding inspired a detailed study on the redox history of uranium in Forsmark in order to determine whether uranium at depth has been recently oxidized, or whether uranium oxidized during an earlier event is exposed to on-going dissolution and re-precipitation in current groundwaters.

3. Methods

3.1. Sample description

For this study, we analyzed uranium minerals from five drillcores. Figs. 1 and 2 show the location of the drillcore sections in the Forsmark bedrock. The relative fracture frequency, which reflects the degree of brittle deformation, is also illustrated. KFM01D (primary uraninite) was collected from the tectonic lens, which showed a lesser extent of brittle deformation and hydrothermal alteration than the binding deformation zones, from which samples KFM04A (primary uraninite, haiweeite, and uranophane), KFR106 (partially coffinitized secondary uraninite), KFM02A (haiweeite and uranophane), and KFR102A (haiweeite and uranophane) were collected. Two thin sections were made from KFR102A, one from a pegmatite in which U(VI) minerals were found in association with primary uranothorite (KFR102A:207B) and one from a vein that contained a mass of uranophane within the same pegmatite (KFR102A:207A).

3.1.1. Uraninite

Although only three samples contained uraninite grains large enough for SIMS analyses, the samples are varied in geological situation, petrographic texture, and chemistry (Fig. 3.a–c). KFM01D contains

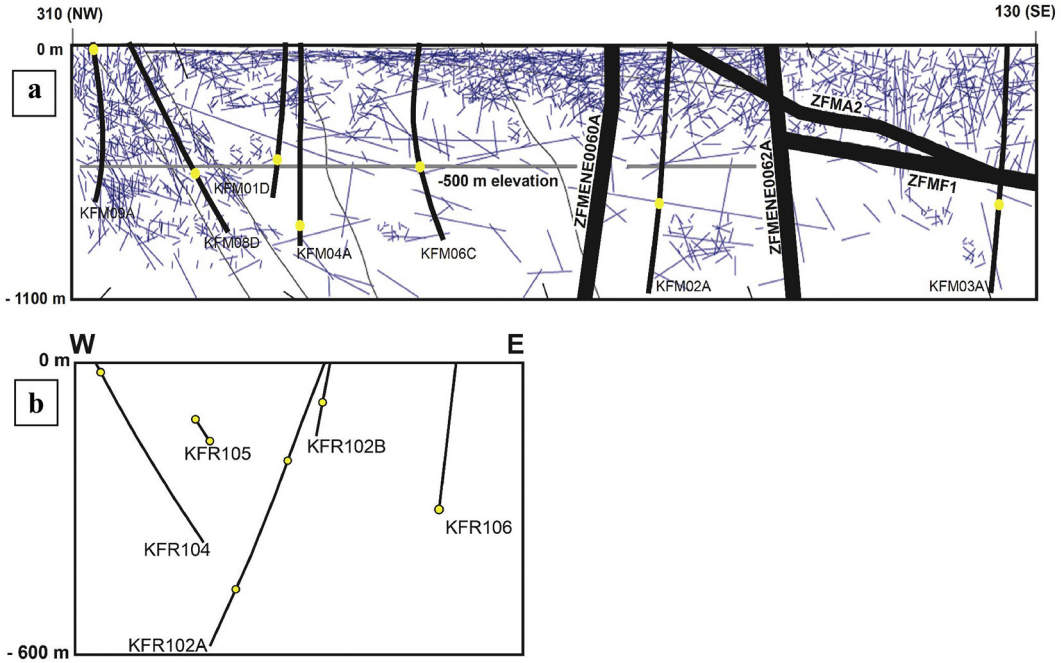

Fig. 2. a–b: Drillcores in which U solids were characterized by Krall et al. (2015) with respect to depth in bedrock. Isotopic data reported from KFM04A, KFM01D, KFR106, and KFR102A. (a) Drillcore samples with respect to relative frequency of hydraulically conductive fractures and major deformation zones. (b) SFR samples with respect to depth. Although a conceptualized fracture network is unavailable for the SFR domain, fracture frequency generally comparable to upper 600 m of Forsmark bedrock.

primary uraninite in a pegmatitic matrix. No evidence of hydrothermal alteration was observed, neither in the form of altered silicates and disseminated hematite throughout the pegmatite matrix nor in the form of Ca-enrichment of the uraninite. KFM04A was taken from a hydrothermally altered pegmatitic matrix containing primary uraninite. In this uraninite, variable enrichment in Ca and depletion in Pb, in addition to minor Si-enrichment, is inferred to be compatible with the chemical signature of early hydrothermal alteration. KFR106 was sampled from a vein in a pegmatite that contained calcite and hematite. The colloform uraninite is partially coffinitized, with areas that are depleted in Pb and enriched in Si. In KFM04A and KFR106, the low SEM-EDS totals (< 90 wt% oxides) and Ca enrichment probably reflect partial oxidation of U(IV) to U(VI) (Sandström et al., 2011). Galena was absent in KFM04A but present in KFM01D and KFR106. All galena grains are < 5 μm across and difficult to analyze for Pb/Pb.

3.1.2. *Haiweeite and uranophane*

The Ca-U(VI)-silicates haiweeite and uranophane commonly coexist in the same thin section sample and are often associated with calcite, which is abundant in fracture mineral generations 2, 3, and 4. EPMA results indicate sub-stoichiometry with respect to uranium. Barium is present in trace amounts in the U(VI) minerals that are closely associated with the primary uraninite or uranothorite, namely in samples KFM04A and KFR102A:207B. In these samples, Ca-U(VI)-silicate minerals are larger than 100 μm. Primary uraninite or uranothorite were not found in samples KFR102A:207A and KFM02A, and the U(VI)-

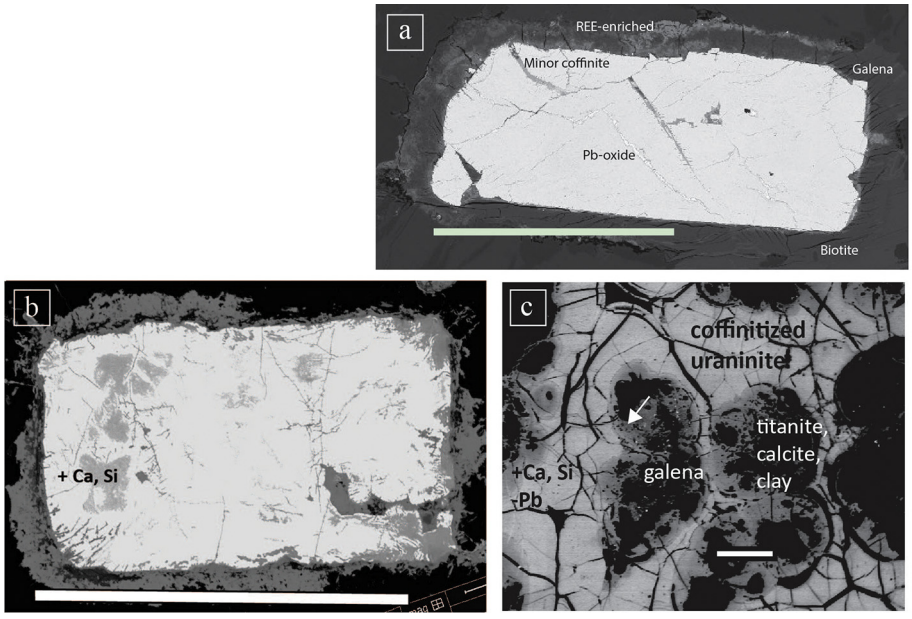

Fig. 3. a–c: Back-scattered electron images showing uraninite textures and element distributions for a) KFM01D, b) KFM04A, and c) KFR106. Unaltered regions shown in bright-grey and altered regions—enriched or depleted in calcium (Ca), silica (Si), and lead (Pb)—in medium-grey, alongside the associated minerals. Scale bar 200 μm.

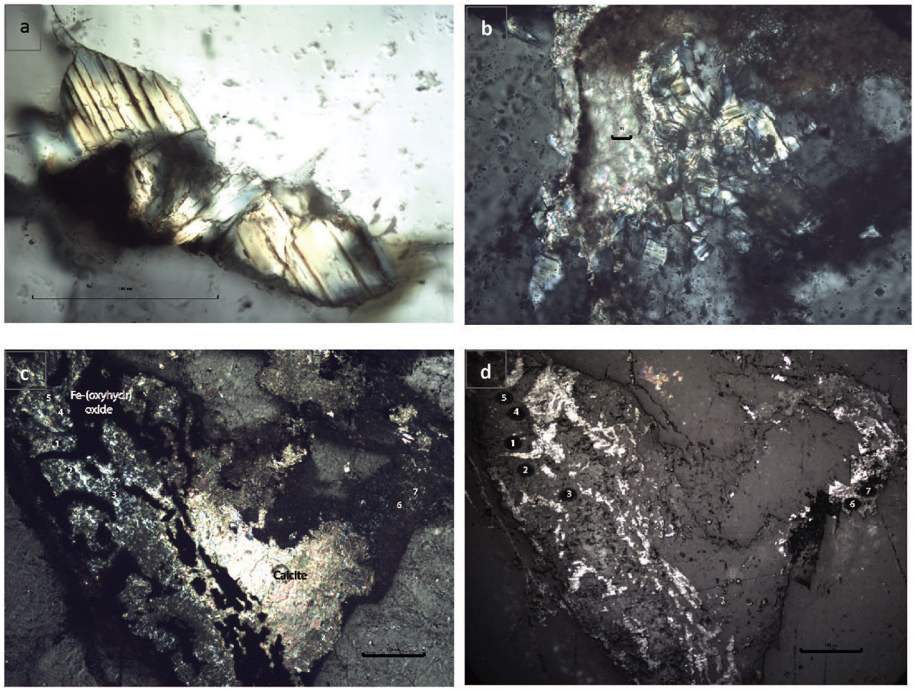

Fig. 4. a–d: Haiweeite and uranophane found in KFM04A (a), KFM02A (b), and KFR102A (c–d). (a) Haiweeite, scale 100 µm. (b) Haiweeite partially replaced by calcite (scale 10 µm). Uranophane overprinted by calcite in KFR102A:207A (grain 2), including spot analyses in (c) cross polarized and (d) reflective light (scale 100 µm).

crystals in these samples were smaller than 50 µm (Fig. 4.a–d). Generation marker minerals such as epidote (generation one), prehnite and laumontite (generation two) were not found in sample KFM04A, but hydrothermal alteration is evident in the form of hematized magnetite, saussuritized plagioclase, calcite, and corrensite. Sample KFM02A contained partially dissolved epidote, in addition to laumontite and calcite. In KFR102A:207A, corrensite, chlorite, and calcite, which are not unique to a single generation, are present (Krall et al., 2015).

3.2. SIMS (uraninite)

Uraninite crystals in gold-coated, mounted thin sections were analyzed for Pb, U, and Th isotopes using a Cameca IMS1280 large-format ion probe at the Nordsim facility, Swedish Museum of Natural History. In order to correct for instrumental mass fractionation, a uraninite standard (P88) was analyzed during the same sessions as the unknowns (Evins et al., 2001). Detailed analytical methods have been described previously for U-Th-Pb (Evins et al., 2001; Whitehouse and Kamber, 2005). A defocused O_2^- primary beam was used to project the image of a 50 µm aperture onto the sample and the primary beam lenses were further tuned to restrict the primary beam current to < 200 pA in order to keep all peaks within the dynamic range of the single ion-counting electron multiplier (EM) detector. Complete U-Th-Pb analyses at a mass resolution (M/DM) of 5400 were performed using a peak switching routine (Evins et al., 2001). A 30 eV energy window was used together with a −50 V sample high voltage offset to sample the low energy tail of the peaks. This offset suppresses the excess signal from a phase so rich in U and minimizes residual orientation and matrix effects relative to the standard. Pb isotopes were corrected for hydride by measuring the $^{208}Pb^1H^+$ peak at nominal mass 209, while non-radiogenic (common) Pb was monitored by measuring ^{204}Pb and subtracted assuming a present-day terrestrial Pb composition according to the model of Stacey and Kramers (1975). U/Pb ratios were calibrated using an empirical power law relationship between Pb^+/U^+ and UO^+/U^+ similar to that used for zircon (Whitehouse et al., 1997). The Pb isotope ratios and ages are presented in Table S1. All uncertainties are reported at the 1σ-level (percent).

3.3. LA-ICP-MS (haiweeite and uranophane)

$^{207}Pb/^{206}Pb$ dating was performed on polished uranophane and haiweeite grains using a NWR193UC excimer laser ablation system coupled to a Nu Instruments AttoM high-resolution inductively coupled plasma mass spectrometer (ICP-MS). The standard U-Th-Pb dating protocol was followed with peak scanning across *m/z* 202, 204, 206, 207, 208, 232, 235 and 238. The ablated sample material was transported from the two-volume 2 laser cell of the NWR system using He at a flow rate of 0.32 l/min. Before putting samples into the mass spectrometer Ar was mixed in at 0.72 l/min. The laser was operated at 5 Hz pulse rate, ~2 J/cm^2 beam energy density and 5 µm spot size. Care was taken to avoid visible cracks and inclusions when determining measurement spots. Unknowns were bracketed with an in-house P88 Uraninite standard (Evins et al., 2001), and an in-house characterized uranophane grain was used as a secondary standard to verify accuracy. Data was reduced offline using Iolite version 2.5 (Paton et al., 2011). The U concentration was too high to measure, so no U/Pb ages could be obtained. Repeat measurements (n = 44) of the secondary uranophane reference as unknowns over the course of the analyses yielded a $^{207}Pb/^{206}Pb$ of 0.1065 (± 6.6%, 2σ), which is in agreement with the solution ICPMS value of 0.1082 (± 0.4%, 2σ). The Pb isotope ratios and ages are presented in Table S1. Uncertainties are reported at the 2σ-level (absolute).

4. Results

Isotope ratios and calculated ages for the suite of U minerals can be found in Table S1, alongside the drillcore name and length, the latter of which corresponds roughly to depth in the bedrock. The crystal chemistry and textural observations from samples KFM01D, KFM04A, KFR102A, and KFM02A are reported in Krall et al., 2015, whereas those of KFR106 are reported in Sandström et al. (2011).

4.1. Uraninite

Results from the analyses of uraninite are presented in Table S1. All uraninite samples produced discordant ages, evident on the Terra-Wasserburg diagrams in Fig. 5.

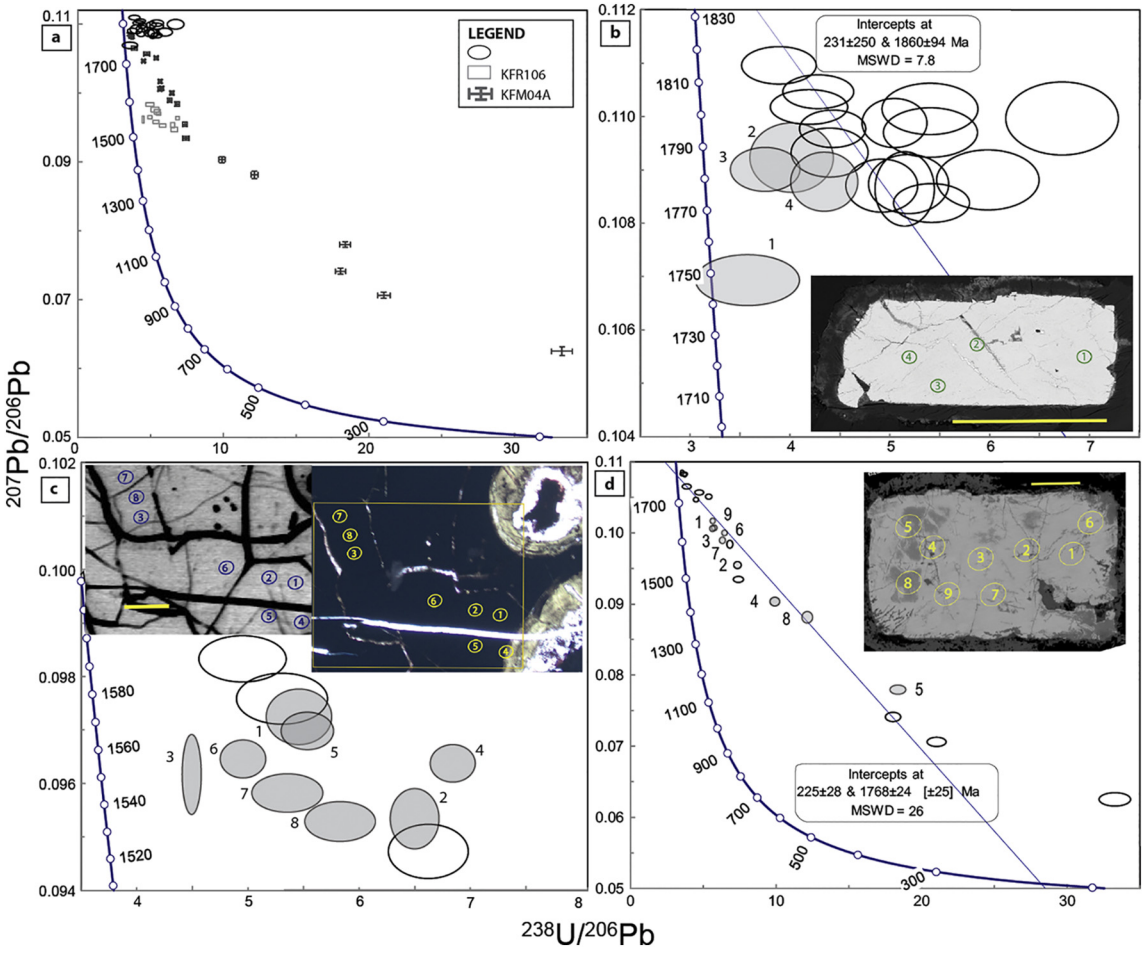

Fig. 5. Pb/Pb and U/Pb ratios from uraninite analyses plotted alongside a Terra-Wasserburg concordia curve. (a) all uraninite samples, (b) KFM01D, (c) KFR106, and (d) KFM04A. Shaded ellipses correspond to the analyses indicated in the mineralogic regions shown in backscattered electron or plane polarized light images.

4.1.1. Formation of primary uraninite

KFM01D is the least discordant sample. One concordant analysis was found at ~1.75 Ga, in an unaltered region that was relatively distant from local fissures (Fig. 5.b; Table 1S, point 1.1). However, analyses near fissures (Fig. S1.1–.4) showed $^{207}Pb/^{206}Pb$ ratios that were greater and $^{206}Pb/^{238}U$ ratios that were less than those from the concordant analysis which are indicative of a depletion in ^{206}Pb. Previously, preferential loss of ^{206}Pb over ^{207}Pb was attributed to a higher rate of ^{222}Rn emanation from the crystal compared to ^{219}Rn due to the longer half-life of ^{222}Rn (~4 d compared to ~4 s; York and Farquhar, 2013).

As calculated from the Wetherill Concordia, no age solution could be found for the analyses from KFM01D. Through the Terra-Wasserburg approach, which differs from the Wetherill approach in that error correlations are neglected, we calculated an age of 1860 ± 94 Ma with an uncertain lower intercept at 231 ± 250 Ma (1σ, MSWD 7.8; Fig. 5.b). A sub-horizontal trend observed in the cluster of analyses, potentially driven by present day diffusion of Pb, biases the regression towards an older age. Since the spread in the $^{207}Pb/^{206}Pb$ ages is limited, the age can be determined through a weighted average approach. Considering only the 50th percentile of $^{207}Pb/^{206}Pb$ ages (older than the median of 1787 ± 7 Ma), the age of the KFM01D uraninite is calculated to 1802 ± 5 Ma (MSWD 3.5). This in good agreement with the age of 1.8 Ga derived from the chemical data following the method of Bowles (1990) (Krall et al., 2015). Overall, the primary, minimally altered uraninite crystals from KFM01D have been dated to 1.8–1.75 Ga and exhibit recent or on-going Pb-loss.

The more altered uraninite grains from KFM04A indicate an age of 1768 ± 24 Ma with a lower intercept at 225 ± 28 Ma (1σ) and an MSWD of 26 (Fig. 5.c). This high MSWD reflects non-analytical scatter (Ludwig, 2000) and highlights the uncertainty of this date particularly due the spread in analyses from the altered regions. If only the unaltered crystals are considered, then the age solution for the initial crystallization of uraninite in KFM04A is refined to 1803 ± 18 Ma, and the MSWD is reduced to 3.7 (1 σ; lower intercept 310 ± 34 Ma). Both the ~1.77 and ~1.8 Ga dates for KFM04A are within the range of 1.8–1.75 Ga for primary uraninite formation as determined from sample KFM01D.

4.1.2. Alteration of primary and precipitation of secondary uraninite

Analyses from uraninite in KFM04A were the most discordant of the three uraninite-bearing samples, particularly in the darker grey regions of the mottled texture revealed by the BSE image (Fig. 5.c). These strongly discordant regions are manifest by substitution of Ca for Pb and low EPMA totals (μ = 92 wt% oxides (Figs. S1.1–.3, S2.3, S4.4–.5, .8; Krall et al., 2015), which collectively indicate the persistence of U (VI) in the uraninite structure (Alberman et al., 1951; Bergman, 1957; Frondel, 1958).

Despite the colloform texture, analyses from KFR106 are not significantly more discordant than the KFM01D analyses (Fig. 5.d). Nevertheless, we found no age solution for the secondary uraninite in this sample. However, the slope and intercepts of the KFR106 results are similar to those of the strongly discordant regions of KFM04A (Fig. 5.a). This which might indicate that the timing of the precipitation of secondary uraninite is similar to that of the alteration of the primary uraninite. If this interpretation is valid, then the event responsible for

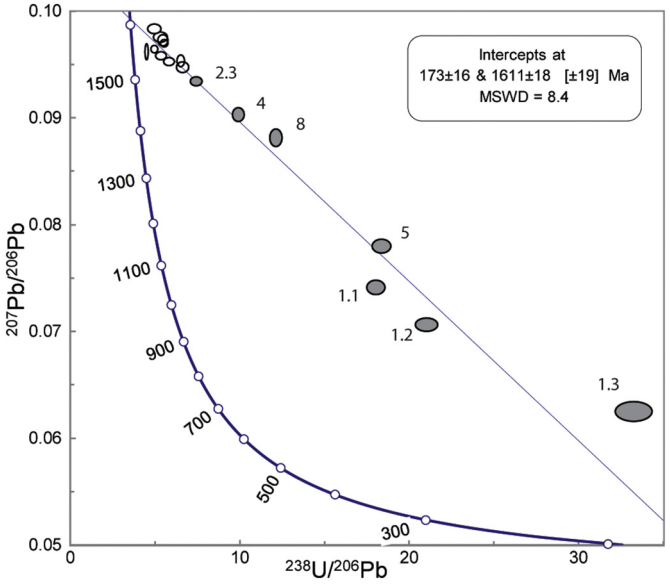

Fig. 6. Terra-Wasserburg diagram showing the age determination if KFR106 (empty ellipse) and the altered regions of KFM04A (grey ellipse) are considered together. Labels for grey data points correspond to points 4, 5, & 8 as marked in Fig. 5.d, as well analyses 1.1–1.3 and 2.3 shown in Table S1 and Fig. S3.1, .2.

the alteration and precipitation occurred at 1611 ± 18 Ma, with a lower intercept of 176 ± 16 Ma (1σ, MSWD 8.4) (Fig. 6).

After initial crystallization of pegmatitic uraninite between 1.8 and 1.75 Ga, secondary uraninite precipitated at ~1.6 Ga, potentially in conjunction with an alteration event that was preserved by the altered, primary uraninite. Lower intercepts range between 350 and 150 Ma, but recent or on-going Pb-loss is also evident in KFM01D. Therefore, the U-Pb system was disrupted at least three times after formation at ~1.8 Ga: 1) ~1.6 Ga, 2) 350–150 Ma, and 3) recently.

4.2. Haiweeite and uranophane

$^{207}Pb/^{206}Pb$ ratios and ages as derived from the analyses of Ca-U (VI)-silicate minerals are presented in Table S1. $^{207}Pb/^{206}Pb$ ages could be derived from samples KFM04A and KFR102A:207B. Major groups are evident between 1.3 and 1.2 Ga (haiweeite in KFM04A; Fig. S3.5, .6) and 400–300 Ma (haiweeite and uranophane in both KFM04A, Fig. S3.7, and KFR102A:207B, Fig. S4.2), and a minor group is apparent at ~1.5 Ga (uranophane in KFR102A:207A). However, samples KFM02A and KFR102A:207A, each of which was partially dissolved by carbonate-rich fluid (Fig. S5, S6), yielded poor ^{207}Pb counting statistics (< 2000 cps) that led to uncertainties of > 20% propagated to the age. Pb counting statistics from the LA-ICP-MS analyses roughly corresponded to the total PbO concentrations up to 5.11, 0.43, 0.19, and 0.13 wt% in KFM04A, KFR102A:207B, KFR102A:207A, and KFM02A, respectively (Krall et al., 2015). Overall, ^{204}Pb activities were scattered around baseline and therefore very low. Thus, the determined $^{207}Pb/^{206}Pb$ ages are reliable without a correction for initial Pb under the assumption that no substantial, early Pb-loss occurred.

4.3. U mineral ages and alteration

Fig. 7, showing the distribution of ^{207}Pb-^{206}Pb ages of uraninite and U(VI)-silicate phases, illustrates the emergence of at least four major U mineral generations:

1. primary pegmatitic uraninite at 1.8–1.75 Ga,
2. secondary uraninite at ~1.6 Ga,
3. Ca-U(VI)-silicates, including haiweeite and uranophane, at 1.3–1.2 Ga,
4. uranophane and haiweeite during the Palaeozoic (400–300 Ma).

5. Discussion

5.1. Proterozoic

The ~1.8 Ga age of the primary uraninite coincides with pegmatite emplacement at Forsmark (Hermansson et al., 2007), while the 1.6 Ga date is within the 1.8–1.1 Ga constraint on the first generation of fracture minerals. However, the 1.3–1.2 Ma group of Ca-U(VI) silicates predates the second episode of hydrothermal fluid circulation, dated to Sveconorwegian (~1100–900 Ma) by Sandström et al. (2009).

5.1.1. Formation and alteration of uraninite

Crystallization of the igneous rocks and ductile deformation of the bedrock at Forsmark occurred between 1.9 and 1.8 Ga (Stephens et al., 2005; Hermansson et al., 2008). Pegmatites formed in several stages, ranging from before to after completion of the ductile deformation (Hermansson et al., 2007). Thus, the 1.8–1.75 Ga timing of uraninite crystallization is compatible with that of the emplacement of local pegmatites.

Furthermore, Welin (1963, 1964, 1992) dated the earliest uraninite occurrence in the Forsmark region to ~1760 Ma, which is similar to the 1768 Ma date derived from the bulk age of the KFM04A uraninite. The previously reported uraninite was found in skarn-hosted iron ore, formed concurrently with pegmatite emplacement, which in some cases was also affected by ductile deformation and hydrothermal alteration (Welin, 1964). For instance, Wilhelm III, the most discordant of the older samples (Fig. 8), was altered and partially replaced by unspecified secondary uranium minerals (Welin, 1963). Thus, similar to KFM04A, some of the skarn-hosted uraninites have probably been partially reset at ~1.6 Ga so that the age of initial formation as derived from the bulk analyses reported by Welin is erroneously young.

Through the high spatial resolution SIMS results, it is possible to discriminate between the precipitation of primary uraninite at ~1.8 Ga, earlier than the 1.76 Ga age determined by Welin (1963) and a Pb-loss episode at ~1.6 Ga. Electron microprobe data shows that this Pb-loss episode was manifest by replacement of Pb with Ca in the KFM04A uraninite (Krall et al., 2015). These divalent cations balance the charge in uraninite that contains some U(VI), described by the formula $(U^{4+}_{1-2y}U^{6+}_{y}M^{2+}_{y})O_2$, where M^{2+} represents a divalent cation. The exchange of Pb for Ca, the latter of which is more compatible in the crystal structure, could indicate that U(VI) was stable under the conditions of hydrothermal alteration. Alternatively, auto-oxidation (i.e. the transfer of electrons from Pb^{4+} to a neighboring U^{4+} and stabilization as Pb^{2+} and U^{6+} following decay of U^{4+}) followed by matrix-diffusion at grain boundaries could explain the persistence of Ca^{2+} and U^{6+} in the uraninite (Bergman, 1957; Frondel, 1958; Janeczek and Ewing, 1992; Fayek et al., 1997; Finch and Murakami, 1999). Even in this latter scenario, a 1.6 Ga Pb-loss episode could still be detected in the discordant data (Fig. 6) if both the hydrothermal alteration and matrix diffusion preferentially affected the grain boundaries.

Precipitation of U(IV) as secondary uraninite in KFR106 contradicts the notion that conditions during the 1.6 Ga event were non-reducing. Although an age solution could not be derived from KFR106 analyses alone, we found an age of 1611 ± 18 Ma from a regression that incorporated the altered regions of primary uraninite from KFM04A. The good agreement between the KFM04A and the KFR106 discordia supports the significance of a 1.6 Ga timing for uraninite alteration (Fig. 8). Furthermore, the texture of sample KFR106 containing secondary uraninite was similar to that for which Welin (1963) determined a discordant age of 1585 Ma, or 1565 Ma if recalculated using updated decay coefficients. Welin (1963) described uraninite-bearing samples from the Betlehem, Kalk, and Norrskedika mines, located within 20 km of the Forsmark site, as partially coffinitized, botryoidal grains

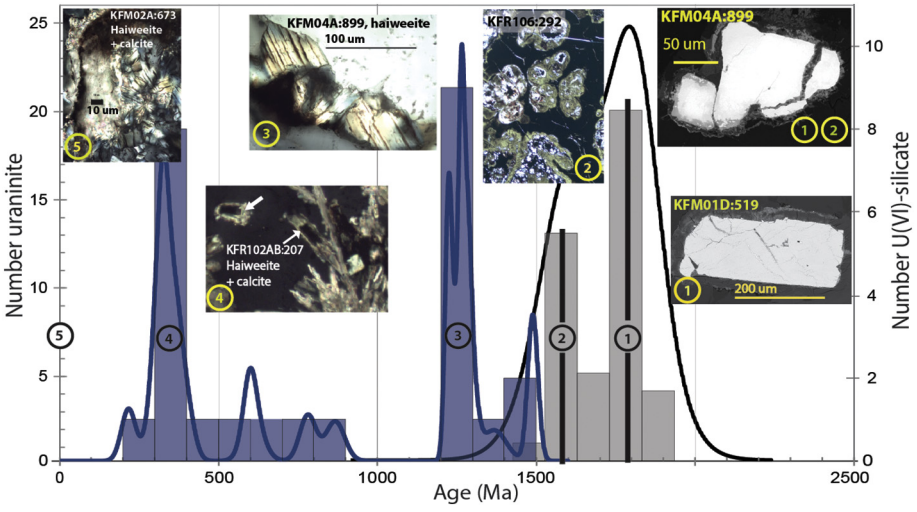

Fig. 7. Relative probably density diagram of $^{207}Pb/^{206}Pb$ ages of uraninite (grey), uranophane and haiweeite (blue). Uraninite analyses are filtered such that only those < 50% discordant are included. Constructed using isoplot (Ludwig, 2000). Images of exemplary crystals from each age group are provided and labelled with a number so as to match the corresponding age group. (For interpretation of the references to color in this figure legend, the reader is referred to the web version of this article.)

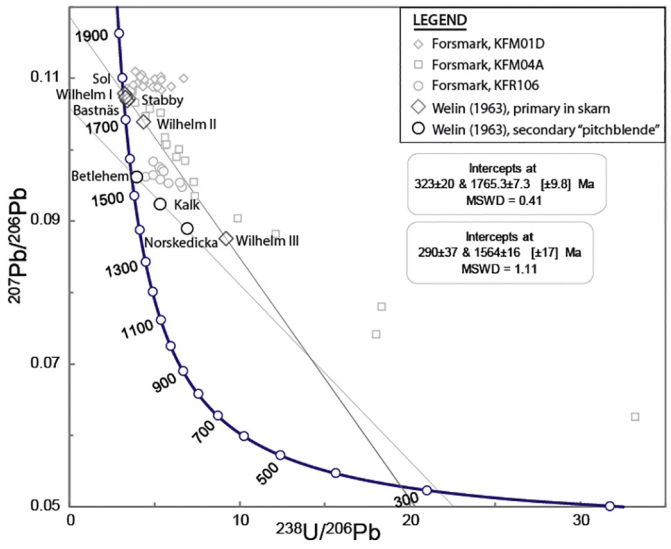

Fig. 8. Analyses and age solutions, recalculated using modern decay coefficients, of uraninite samples collected from iron mines near Forsmark (Welin, 1963) shown alongside recent analyses of uraninite from Forsmark.

associated with hematite and sulfide minerals within veins of calcite, chlorite, and quartz (Welin, 1963). This description is consistent with that of Sandström et al. (2009) for the KFR106 uraninite.

5.1.2. Tectonothermal setting

On the basis of Ar-Ar dating, the timing of the first event of hydrothermal fluid circulation was constrained to 1.8–1.1 Ga, during either a late stage of the Svecokarelian orogeny (1.8–1.7 Ga; Gorbatschev, 2004) or as a far-field effect of the Gothian orogeny (1.7–1.55 Ga; Connelly and Åhäll, 1996; Åhäll and Gower, 1997, Sandström et al., 2009). Welin (1992) further noted a potential relation to the emplacement of the major rapakivi massif of the Åland Iles, situated fewer than 100 km from Forsmark, at 1.57 Ga (Heinonen et al., 2010). However, our results show that alteration and precipitation of the Forsmark uraninite occurred at 1611 ± 18 Ma, which is earlier than the emplacement of the Åland massif and therefore more consistent with a Gothian timing at 1.7–1.55 Ga. On the basis of the orientation of the consequent fracture mineralization relative to that of bulk crustal shortening, Stephens et al. (2007) also proposed a Gothian timing for the first event of hydrothermal fluid circulation.

Relatively concordant results from KFM01D uraninite can also be understood in the context of regional tectonothermal events and local hydrothermal alteration. The tectonic lens at the Forsmark site, from which KFM01D was sampled, has a lower fracture frequency than the deformation zones by which it is bound. Hydrothermal alteration was less pervasive within this lens, and the KFM01D pegmatite matrix, like the uraninite, showed no mineralogic or chemical evidence of alteration. Although discordant analyses in this sample were found, these were not accompanied by chemical exchange that supported structural U(VI), as through hydrothermal alteration or matrix diffusion.

5.1.3. Appearance of Ca-U(VI)-silicate minerals

Ca-U(VI)-silicates appeared in Forsmark after the first event of hydrothermal fluid migration, which was responsible for alteration of primary uraninite and precipitation of secondary uraninite in fractures. Uranophane was dated to 1.4–1.3 Ga (KFR102A:207A) and haiweeite and uranophane are associated with altered pegmatitic uraninite in KFM04A dated at 1.3–1.2 Ga. These ages are younger than the Sveconorwegian age of the generation two K-feldspar as derived from Ar-Ar dating (1.1–1.0 Ga). However, given the tendency of this feldspar to occur along the major deformation zones, which were reactivated during consecutive tectonic events (Stephens et al., 2007; Sandström et al. (2009) noted that the Ar-system in pre-existing feldspar, precipitated at ~1.3 Ga, for instance, may have been reset during the Sveconorwegian orogeny.

One notable pre-Sveconorwegian event that occurred close to Forsmark is the intrusion of the Central Scandinavian Dolerite Group at ~1250 Ma (Söderlund et al., 2006). The regional importance of these post-Jotnian dolerite dikes was also noted by Welin (1992). It is possible that a Sveconorwegian resetting of the Ar-system in K-feldspar masked the effects of this earlier event of regional magmatism. Söderlund et al. (2006) reported U-Pb ages of 1259–1256 Ma in baddeleyite from the Satakunta complex, which includes two dikes in the Swedish towns of Mackmyra and Furuvik located ~50 km from Forsmark. The 1.3–1.2 Ga Pb-Pb ages in haiweeite (KFM04A) are similar to the ages of these dikes. Furthermore, these haiweeite grains precipitated in microfractures within the KFM04A pegmatite (Fig. S3.5, .6). Dike intrusion implies an extensional tectonic setting, which would be accompanied by formation and reactivation of fractures. Such void space probably facilitated the transportation of U(VI) away from earlier-formed minerals, evidenced in KFM04A. Therefore, it is likely that Forsmark has been affected by an additional tectonothermal event, which predated the Sveconorwegian orogeny and was responsible for the precipitation of Ca-U(VI)-silicates.

5.2. Palaeozoic

Haiweeite and uranophane also reveal Palaeozoic Pb-Pb ages

(400–300 Ma; KFM04A and KFR102A). While these ages are compatible with the third major event of hydrothermal fluid circulation at Forsmark, the precipitation of U(VI)-minerals during this event is unexpected. The geochemical conditions, as evidenced by the contemporaneous precipitation of sulfide minerals pyrite and galena, were strongly reducing (Sandström et al., 2009) and would seem to favor reduction of U(VI) to U(IV).

Reducing conditions prevailed during the Palaeozoic due to emanation of fluids from an organic-rich sedimentary sequence that covered the crystalline basement (Sandström et al., 2006). These fluids supplied organic carbon that fed sulfate-reducing bacteria (Drake et al., 2017b). Mixing between the organic-rich fluids and basement brines promoted mineralization. The presence of asphaltite, a naturally occurring bitumen, proved that this fracture mineral generation had a carbon-rich fluid source from sedimentary rocks (Sandström et al., 2006). Asphaltite is abundant at depths < 150 m.b.s.l., but near the Forsmark deformation zone it has been found as deep as 400 m.b.s.l. Otherwise, Palaeozoic fracture minerals are most common in the upper 350 m of the bedrock (Sandström et al., 2009; Sandström et al., 2006). Welin (1966b) described the co-occurrence of asphaltite and thucolite, the latter of which denotes the presence of U with the organic material, at several sites in Sweden. Where the uranium minerals were influenced by organic material, thucolite was found alongside the primary U minerals.

Of the tertiary U phases, Ca-U(VI)-silicate minerals are most common below 200 m.b.s.l., whereas above 200 m.b.s.l. and outside of the major deformation zones, Si-rich mixed U(IV)-U(VI) oxides (< 10 μm grains) are deposited on Fe(Al)-silicates, sometimes in association with galena (Krall et al., 2015). Therefore, Ca-U(VI)-silicates in pegmatites and in some areas of the fracture network may have been isolated from the highly reducing fluids responsible for Palaeozoic minerals (generation 3). Since the hydrostatic pressure exerted by the Caledonian foreland basin created and reactivated fractures during the Palaeozoic (Sandström et al., 2009 and references therein), circulation of hydrothermal fluids was probably pervasive throughout the Forsmark fracture network during this period. However, heterogeneity in fluid character and composition is evident (Drake et al., 2017b). Circulation of basement fluids, which did not mix with the organic-rich fluids, may have promoted uranophane precipitation in the deeper extents of the Forsmark fracture network during the Palaeozoic. This interpretation is supported by the absence of sulfide minerals, asphaltite, and thucolite in Palaeozoic samples with uranophane and haiweeite.

5.3. Recent recrystallization or alteration

Pb concentrations in the majority of uranophane and haiweeite grains in KFR102A:207A and KFM02A:673 that are too low to allow us to calculate an age. Nevertheless, such low Pb concentrations are compatible with recent (100 Ma to present day) (re)crystallization of uranophane and haiweeite or enhanced Pb loss from these minerals. Even where the age in KFR102A:207A could be calculated to 1367 ± 76 Ma, Pb concentrations could be low (2060 cps ^{207}Pb) relative to those in the younger Palaeozoic uranophane of KFM04A and KFR102A:207B (9000 ± 5700 cps ^{207}Pb). Although most ages from samples KFM02A and KFR102A:207A are unreliable, the low Pb concentrations imply that these samples have been more recently affected by fluids than samples KFM04A and KFR102A:207B.

Uranophane and haiweeite crystals characterized by low Pb concentrations in KFR102A:207A and KFM02A have been altered by carbonate-bearing fluids (Fig. 4.b–d). Calcite precipitated during the Proterozoic and Palaeozoic circulation of hydrothermal fluids. However, groundwaters currently in the fracture network are also at the solubility limit with respect to calcite (Gimeno et al., 2008), and these groundwaters are strongly undersaturated with respect to uranophane (Krall et al., 2017). Low Pb concentrations may reflect on-going interaction between U(VI) minerals and groundwaters in some areas of the fracture network.

5.4. Palaeoredox behavior of uranium

The presence of > 300 Ma uranyl silicates, haiweeite and uranophane, in the deep fracture network of the Forsmark site, is surprising considering the availability of reductants in the current groundwater. Since uranyl minerals often form as a result of near-surface weathering of older U minerals, it is uncommon to find uranyl silicates older than 1 Ma. However, several occurrences have been reported from the Scandinavian shield. Löfvendahl and Holm (1981) found uranophane in secular equilibrium (i.e. > 1 Ma), while Löfendahl and Åberg (1982) found kasolite, a Pb-U(VI)-silicate, that produced concordant U-Pb ages of ~1750 Ma. In addition, the uranophane standard analyzed in this study produced a Pb-Pb age of ~1.7 Ga. If the Forsmark Ca-U(VI)-silicates had formed from local uraninite that was corroded by post-glacial meltwaters during the Holocene and simply inherited the Pb-signature from the uraninite (~0.10) mixed with the ^{207}Pb/^{206}Pb of recent common Pb, then a broad range of ^{207}Pb/^{206}Pb would be expected. However, the observed values are lower and cluster around ~0.08 and ~0.05. Therefore, the present results support a ~1250 Ma oxidation of U(IV) to U(VI) at Forsmark in connection to regional geological events, particularly in the bedrock domains affected by brittle deformation.

Given the relations between the Ca-U(VI)-ages and regional geologic events around Forsmark, it is likely that some process has facilitated a geologically early oxidation of the local U(IV) and that the persistence of these Ca-U(VI)-silicates in the current geochemical regime is remarkable. The Palaeozoic age of uranophane and haiweeite also implies that U(VI), where bound in mineral structures, may endure in certain bedrock localities when geologic fluids in other parts of the fracture network are strongly reducing.

5.4.1. Mechanisms of U(IV) oxidation

At temperatures prevalent during the two Proterozoic events of hydrothermal fluid circulation (150°–300 °C; Sandström et al., 2009), O_2 should be required to support the hematization of magnetite (Kojima et al., 1994), a characteristic reaction of these episodes. Although a source of O_2 to the deep hydrothermal fluids remains unknown, some O_2 may have been available to oxidize the U(IV) during these early episodes. However, it is not clear whether U(IV) was oxidized during the Gothian hydrothermal event. Altered regions of KFM04A and KFR106 uraninite contained appreciable concentrations of Ca (6–13 wt % CaO), which can replace radiogenic Pb^{2+} and indicate the presence of U(VI), and were date to ~1.6 Ga, but it is not clear whether the U(VI) should be attributed to the hydrothermal fluids or to auto-oxidation (Section 5.1.1). Given that the KFM04A pegmatite was influenced by several subsequent hydrothermal episodes, this question cannot be resolved using our discordant data alone.

Fluid alkalinity and the availability of complexing ligand HCO_3^- were higher during the second Proterozoic hydrothermal episode, responsible for the mobilization and reprecipitation of U(VI) in Ca-U(VI)-silicates, dated to 1.3–1.2 Ga, within micro-fractures (Fig. S3.5, .6). Cogenetic hematite and calcite suggest that conditions were oxidizing and alkaline during this stage of tectonothermal evolution. The hydrothermal fluid temperatures ranged from 150° to 250 °C. Within the range of 100 to 200 °C in the hematite stability field, U(VI)-carbonate complexes can predominate the speciation of aqueous U at pH as low as 6 (Kojima et al., 1994). Therefore, it is likely that mobilization of U(VI), oxidized during episodic hydrothermal fluid circulation or auto-oxidation during the Proterozoic, was facilitated by aqueous U(VI)-carbonate complexes.

5.4.2. Maintenance of U(VI) in reducing environments

On the basis of equilibrium thermodynamics, the persistence of Ca-

U(VI)-silicates of Proterozoic origin is unexpected in the current geochemical regime, given the groundwater Fe(II) and S(-II) contents (Krall et al., 2017). Furthermore, these minerals survived and precipitated during the Palaeozoic era, which was otherwise marked by reducing conditions and sulfide mineral precipitation. These observations can be attributed to the heterogeneity of the Forsmark fracture network throughout its tectonothermal, and consequentially geochemical, evolution.

Uraninite in the minimally fractured tectonic lens is the most pristine zone studied (KFM01D). In this stable setting, absent of major deformation zones and associated fractures, the uraninite shows no textural, chemical, or isotopic evidence of alteration by hydrothermal fluids. In contrast, hydrothermal fluids appear to have altered primary uraninite and caused precipitation of secondary, botryoidal uraninite at ~1.6 Ga.

A hydrothermal episode that occurred later during the Proterozoic, in conjunction with extensional tectonics, was responsible for precipitation of Ca-U(VI)-silicates after U was transported, potentially as aqueous U(VI)-carbonate complexes. However, evidence for this event is found in only some of the samples. For instance, U(VI)-minerals dated to 1.3–1.2 Ga were present alongside altered uraninite in KFM04A, while traces of this episode, in the form of U(VI)-minerals or a ~1.25 Ma age determination, were absent from the U(IV)-bearing secondary uraninite in KFR106. This suggests that bedrock exposure to hydrothermal fluids, along with their associated redox components, was scattered throughout the site.

Oxidation of U(IV) during Proterozoic hydrothermal alteration is supported by contemporaneous oxidation of Fe and deposition of Fe (III)-minerals (Section 5.4.1); however, the precipitation of U(VI) minerals (e.g. samples KFM04A (900 m.b.s.l.) and KFR102AB (200 m.b.s.l.)) during the reducing geochemical conditions of the Palaeozoic warrants further explanation. Since uranium oxidized during the Proterozoic persists to this day within uranophane and haiweeite, these minerals also represent U(VI) sources to Palaeozoic fluids. As indicated by abundant calcite that precipitated during this time (Drake et al., 2017b), Palaeozoic fluids were rich in (bi)carbonate, a strong complexing ligand for U(VI). Although the precipitation of Palaeozoic asphaltite and sulfides indicate that conditions were also strongly reducing, the abundance of these minerals diminished at depths below 400 m.b.s.l. in the current regime (Sandström et al., 2009). The organic carbon for the asphaltite and sulfide minerals, the latter of which formed after consumption of organic carbon by sulfate-reducing bacteria (Drake et al., 2017b), was injected downward into the fracture network from the overlying Caledonian Foreland Basin (Sandström et al., 2009). Thus, redox conditions varied throughout the fracture network, while the availability of (bi)carbonate, which may complex with U(VI) and inhibit its reduction, was relatively pervasive. Therefore, U(VI) may have predominated relative to U(IV) where alkalinity was high but organic carbon was unavailable to generate U(VI) reductants, such as sulfide. These conditions occurred irregularly throughout the fracture network, but spatial variation in aqueous geochemistry during the Palaeozoic is one explanation for the precipitation of uranyl minerals during this time.

Fractures active during the Proterozoic were largely sealed by the precipitation of hydrothermal minerals, although some were reactivated during and after the Palaeozoic (Drake et al., 2017b). Thus, certain Ca-U(VI)-silicate depositions may have been isolated from reactive Palaeozoic fluids, thereby impeding the reduction of U(VI). Nevertheless, fractures that are conductive at present may intersect the Proterozoic fractures. Overall, the fracture regime as a conduit for geologic fluids has imparted an important control on the spatial evolution of the Forsmark redox conditions.

6. Conclusions

Through U-Pb isotope analyses of U(IV) and U(VI) minerals, we have deciphered the response of the U redox system to a thermochemical spectrum of geologic fluids. A chronology of the tectonothermal evolution of the Fennoscandian shield can be refined on the basis of U-mineral ages.

The isotope systems within uranium minerals were disrupted during the Gothian orogeny at ~1.6 Ga. This age is more precise than the 1.8–1.1 Ga range reported by Sandström et al. (2009) and similar to the ~1.56 Ga date provided by Welin (1963). Ca-U(VI)-silicates began to precipitate at ~1.25 Ga, contemporaneous with the emplacement of dikes from the Central Scandinavian Dolerite Group. At Forsmark, this event was apparently overprinted by a hydrothermal episode during the Sveconorwegian orogeny (1.1–0.9 Ga; Sandström et al., 2009). Palaeozoic ages (400–300 Ma) derived from a suite of uranophane and haiweeite are similar to those of a third hydrothermal event dated to 456–277 Ma by Sandström et al. (2009). U(VI) originally oxidized during the Proterozoic may have persisted through the Palaeozoic if retained in the matrix of U(VI)-minerals. Finally, low Pb-contents in Ca-U(VI)-silicate minerals indicate recent or on-going interaction between these minerals and carbonate-rich fluids.

The observed heterogeneity in U redox conditions throughout the fracture network during the various episodes of hydrothermal fluid circulation has implications on the redox evolution of fractured crystalline bedrock. That each fracture locality carries a unique history of water-rock interaction is important to consider in the interpretation of present-day groundwater geochemistry, which likewise shows variation in Eh and alkalinity. Our results should inform future studies that use Ra isotopes and geochemical modelling to further address the variability in aqueous U concentrations in groundwaters at Forsmark and the SFR.

Supplementary data to this article can be found online at https://doi.org/10.1016/j.chemgeo.2018.12.013.

Acknowledgements

We are grateful to R.J. Finch for his review of this paper. We also thank Kerstin Linden, Melanie Schmitt, and Jeremy Bellucci for their assistance with sample preparation and the SIMS and LA-ICP-MS analyses. This study was supported by the Swedish Nuclear Fuel and Waste Management Company and the European Union Seventh Framework Programme for research, technological development and demonstration under Grant Agreement No. 290336 and is Vegacenter publication #013.

References

Åhäll, K.-I., Gower, C.F., 1997. The Gothian and Labradorian orogens: variations in accretionary tectonism along a late Paleoproterozoic Laurentia–Baltica margin. GFF 119, 181–191.
Åhäll, K.-I., Larson, S.Å., 2000. Growth-related 1.85–1.55 Ga magmatism in the Baltic Shield; a review addressing the tectonic characteristics of Svecofennian, TIB 1-related, and Gothian events. GFF 122 (2), 193–206.
Alberman, K.B., Blakely, R.C., Anderson, J.S., 1951. The oxides of uranium—part II, binary system UO2–CaO. J. Chem. Soc. 1352–1356.
Bergman, R.M., 1957. The role of lead and excess oxygen in uraninite. Am. Mineral. 42, 705–731.
Bingen, B., Nordgulen, Ø., Viola, G., 2008. A four-phase model for the Sveconorwegian orogeny, SW Scandinavia. Nor. J. Geol. 88, 43–72.
Bowles, J., 1990. Age dating of individual grains of uraninite in rocks from electron microprobe analyses. Chem. Geol. 83, 47–53.
Cederbom, C., Larson, S.Å., Tullborg, E.-L., Stiberg, J.-P., 2000. Fission track thermochronology applied to Phanerozoic thermotectonic events in central and southern Sweden. Tectonophysics 316, 153–167.
Christoffel, A.A., Connelly, J.N., Åhäll, K.-I., 1999. Timing and characterization of recurrent pre-Sveconorwegian metamorphism and deformation in the Varberg–Halmstad region of SW Sweden. Precambrian Res. 98, 173–195.
Connelly, J.N., Åhäll, K.-I., 1996. The mid-Proterozoic cratonisation of Laurentia–Baltica; new age constraints from SW Sweden. Geol. Soc. Lond. Spec. Publ. 112, 261–273.
Drake, H., Suksi, J., Tullborg, E.-L., Lahaye, Y., 2017a. Quaternary redox transitions in deep crystalline rock fractures at the western margin of the Greenland ice sheet. Appl. Geochem. 76, 196–209.
Drake, H., Heim, C., Whitehouse, M., Broman, C., Åström, M., 2017b. Episodic methanogenesis, methane oxidation and sulphate reduction in deep granite fractures at

Forsmark, Sweden. Procedia Earth Planet. Sci. 17, 702–705.
Evins, L.Z., Sunde, T., Fayek, M., Schöberg, H., 2001. U and Pb Isotope Analysis of Uraninite and Galena by Ion Microprobe. Technical Report TR-01-35. SKB.
Fayek, M., Janeczek, J., Ewing, R.C., 1997. Mineral chemistry and oxygen isotopic analyses of uraninite, pitchblende and uranium alteration minerals from the Cigar Lake deposit, Saskatchewan, Canada. Appl. Geochem. 12 (5), 549–565.
Finch, R., Murakami, T., 1999. Systematics and paragenesis of uranium minerals. Rev. Mineral. 38, 91–180.
Frondel, C., 1958. Systematic mineralogy of uranium and thorium. U.S. Geol. Surv. Bull. 1064.
Gee, D.G., Sturt, B.A., 1985. The Caledonide Orogen–Scandinavia and Related Areas. Wiley, Chichester, UK.
Gimeno, M.J., Auqué, L.F., Gómez, J.B., Acero, P., 2008. Water–Rock Interaction Modelling and Uncertainties of Mixing Modelling. SKB Report R-08-86. Swedish Nuclear Fuel and Waste Management Company. www.skb.se.
Gorbatschev, R., 2004. The Transscandinavian Igneous Belt — introduction and background. In: Special Paper — Geological Survey of Finland 37, pp. 9–15.
Haapala, I., Rämö, O.T., Frindt, S., 2005. Comparison of Proterozoic and Phanerozoic rift-related basaltic–granitic magmatism. Lithos 80, 1–32.
Heinonen, A.P., Andersen, T., Rämö, O.T., 2010. Re-evaluation of rapakivi petrogenesis: source constraints from the Hf isotope composition of zircon in the rapakivi granites and associated mafic rocks of southern Finland. J. Petrol. 51 (8), 1687–1709. https://doi.org/10.1093/petrology/egq035.
Hermansson, T., Stephens, M.B., Corfu, F., Page, L., Andersson, J., 2007. Penetrative ductile deformation and amphibolites-facies metamorphism prior to 1851 Ma in the western part of the Svecofennian orogen, Fennoscandian Shield. Precambrian Res. 153, 29–45.
Hermansson, T., Stephens, M.B., Corfu, F., Page, L.M., Andersson, J., 2008. Migratory tectonic switching, western Svecofennian orogen, central Sweden: constrains from U/Pb zircon and titanite geochronology. Precambrian Res. 161, 250–278.
Hogmalm, J., Söderlund, U., Larson, S.Å., Claeson, D., 2006. The Ulvö Gabbro Complex of the 1.27–1.25 Ga Central Scandinavian Dolerite Group (CSDG); intrusive age, magmatic setting and metamorphic history. GFF 128 (1), 1–6.
Hubbard, F.H., 1975. The Precambrian crystalline complex of south-western Sweden. The geology and petrogenetic development of the Varberg Region. Geol. Fören. Stockh. Förh. 97, 223–236.
Janeczek, J., Ewing, R.C., 1992. Dissolution and alteration of uraninite under reducing conditions. J. Nucl. Mater. 190, 157–173.
Kojima, S., Takeda, S., Kogita, S., 1994. Chemical factors controlling the solubility of uraninite and their significance in the genesis of unconformity-related uranium deposits. Mineral. Deposita 29 (4), 353–360.
Krall, L., Sandström, B., Tullborg, E.-L., Evins, L.Z., 2015. Natural uranium in Forsmark, Sweden: the solid phase. Appl. Geochem. 59, 178–188.
Krall, L., Auque, L., Tullborg, E.-L., Suksi, J., Trezzi, G., Garcia-Orellana, J., Andersson, P., Porcelli, D., 2017. Tracing U mobility in deep groundwater using Ra isotopes. Procedia Earth Planet. Sci. 17, 484–487.
Laaksoharju, M., Smellie, J., Tullborg, E.-L., 2008. Bedrock Hydrogeochemistry Forsmark, Site Descriptive Modelling Forsmark. SKB R-08-47. Svensk Kärnbränslehantering AB.
Larson, S.Å., Berglund, J., 1992. A chronological subdivision of the Transscandinavian Igneous Belt – three magmatic episodes? Geol. Fören. Stockh. Förh. 114 (4), 459–461.
Löfendahl, R., Åberg, G., 1982. An isotope study of Swedish secondary U-Pb minerals. Geologiska Röenengen i Stockholm Förhandlingar 103 (3), 331–342.
Löfvendahl, R., Holm, E., 1981. Radioactive disequilibria and apparent ages of secondary uranium minerals from Sweden. Lithos 14 (3), 189–201.
Ludwig, K.R., 2000. User's manual for Isoplot/Ex version 2.4. In: Special Publication No. 1a. Berkeley Geochronology Center.
Möller, C., Andersson, J., Lundqvist, I., Hellström, F., 2007. Linking deformation, migmatite formation and zircon U–Pb geochronology in poly-metamophic orthogneisses, Sveconorwegian Province, Sweden. J. Metamorph. Geol. 25, 727–750.
Näslund, J.O., Brandefelt, J., Liljedahl, L.C., 2013. Climate considerations in long-term safety assessments for nuclear waste repositories. Ambio 42 (4), 393–401.
Paton, C., Hellstrom, J., Paul, B., Woodhead, J., Hergt, J., 2011. Iolite: freeware for the visualisation and processing of mass spectrometric data. J. Anal. At. Spectrom. 26, 2508–2518.
Roberts, D., 2003. The Scandinavian Caledonides; event chronology, palaeogeographic settings and likely modern analogues. Tectonophysics 365, 283–299.
Saintot, A., Stephens, M.B., Viola, G., Nordgulen, Ø., 2011. Brittle tectonic evolution and paleostress field reconstruction in the southwestern part of the Fennoscandian Shield, Forsmark, Sweden. Tectonics 30, TC4002. https://doi.org/10.1029/2010TC002781.
Sandström, B., Tullborg, E.-L., De Torres, T., Ortiz, J.E., 2006. The occurrence and potential origin of asphaltite in bedrock fractures, Forsmark, central Sweden. GFF 128, 233–242.
Sandström, B., Tullborg, E.-L., Smellie, J., MacKenzie, A., Suksi, J., 2008. Fracture Mineralogy of the Forsmark. SKB R-Report R-08-102. SKB, Stockholm, Sweden.
Sandström, B., Tullborg, E.-L., Larson, S.A., Page, L., 2009. Brittle tectonothermal evolution in the Forsmark area, central Fennoscandian Shield, recorded by paragenesis, orientation and 40Ar/39Ar geochronology of fracture minerals. Tectonophysics 478, 158–174.
Sandström, B., Nilsson, K., Tullborg, E.-L., 2011. Fracture Mineralogy Including Identification of Uranium Phases and Hydrogeochemical Characterization of Groundwater in Borehole KFR106. SKB P-Report P-11-41. SKB, Stockholm, Sweden.
SKB, 2008. Site Description of Forsmark at Completion of the Site Investigation Phase. SKB TR-08-05. Swedish Nuclear Fuel and Waste Management Co., Stockholm, Sweden.
Smellie, J., Tullborg, E.-L., Nilsson, A.-C., 2008. Explorative Analysis of Major Components and Isotopes. SKB-R-08-84. Swedish Nuclear Fuel and Waste Management Co., Stockholm, Sweden.
Söderlund, U., Isachsen, C.E., Bylund, G., Heaman, L.M., Patchett, P.J., Vervoort, J.D., Andersson, U.B., 2005. U–Pb baddeleyite ages and Hf, Nd isotope chemistry constraining repeated mafic magmatism in the Fennoscandian Shield from 1.6 to 0.9 Ga. Contrib. Mineral. Petrol. 150, 174–194.
Söderlund, U., Elming, S.-Å., Ernst, R.E., Schissel, D., 2006. The Central Scandinavian Dolerite Group—protracted hotspot activity or back-arc magmatism? Constraints from U-Pb baddeleyite geochronology and Hf isotopic data. Precambrian Res. 150, 136–152.
Söderlund, P., Hermansson, T., Page, L.M., Stephens, M.B., 2008. Biotite and muscovite $^{40}Ar/^{39}Ar$ geochronological constraints on the post-Svecofennian tectonothermal evolution, Forsmark site, central Sweden. Int. J. Earth Sci. https://doi.org/10.1007/s00531-008-0346-8.
Stacey, J.S., Kramers, J.D., 1975. Approximation of terrestrial lead isotope evolution by a 2-stage model. Earth Planet. Sci. Lett. 26 (2), 207–221.
Stephens, M.B., Andersson, J., 2015. Migmatization related to mafic underplating and intra- or back-arc spreading above a subduction boundary in a 2.0–1.8 Ga accretionary orogen, Sweden. Precambrian Res. 264, 235–237.
Stephens, M.B., Lundqvist, S., Bergman, T., Ekstrom, M., 2005. Forsmark Site Investigation. Bedrock Mapping. Petrographic and Geochemical Characteristics of Rock Types Based on Stage 1 (2002) and Stage 2 (2003) Surface Data. SKB Report P-04-08. Swedish Nuclear Fuel and Waste Management Company, Stockholm, Sweden.
Stephens, M.B., Fox, A., La Pointe, P.R., Simeonov, A., Isaksson, H., Hermansson, J., Öhman, J., 2007. Geology Forsmark. Site Descriptive Modelling Forsmark Stage 2.2. SKB Report R-07-45. Swedish Nuclear Fuel and Waste Management Company, Stockholm, Sweden.
Suksi, J., Rasilainen, K., Casanova, J., Ruskeeniemi, T., Blomqvist, R., Smellie, J.A.T., 2001. U-series disequilibria in a groundwater flow route as an indicator of uranium migration processes. J. Contam. Hydrol. 47 (2), 187–196.
Tullborg, E.-L., Suksi, J., Geipel, G., Krall, L., Auqué, L., Gimeno, M., Puigdomenech, I., 2017. The occurrences of Ca2UO2(CO3)3 complex in Fe(II) containing deep groundwater at Forsmark, Eastern Sweden. Procedia Earth Planet. Sci. 17, 440–443.
Welin, E., 1963. The interpretation of discordant U/Pb age data from central Sweden. GFF 85 (2), 223–235. https://doi.org/10.1080/11035896309448886.
Welin, E., 1964. Uranium disseminations and vein fillings in iron ores of northern Uppland, central Sweden. GFF 86, 51–82.
Welin, E., 1966a. Uranium mineralizations and age relationships in the Precambrian bedrock of central and southeastern Sweden. GFF 88 (1), 34–67. https://doi.org/10.1080/11035896609448333.
Welin, E., 1966b. The occurrence of asphaltite and thucholite in the Precambrian bedrock of Sweden. GFF 87, 509–526.
Welin, E., 1980. Tabulation of recalculated radiometric ages published 1960–1979 for rocks and minerals in Sweden. GFF 101 (4), 309–320. https://doi.org/10.1080/11035898009450850.
Welin, E., 1992. Isotopic results of the Proterozoic crustal evolution of south-central Sweden; review and conclusions. GFF 114 (3), 299–312. https://doi.org/10.1080/11035899209454791.
Whitehouse, M.J., Kamber, B.S., 2005. Assigning dates to thin gneissic veins in high-grade metamorphic terranes: a cautionary tale from Akilia, southwest Greenland. J. Petrol. 46, 291–318.
Whitehouse, M.J., Claesson, S., Sunde, T., Vestin, J., 1997. Ion-microprobe U–Pb zircon geochronology and correlation of Archaean gneisses from the Lewisian Complex of Gruinard Bay, north-west Scotland. Geochim. Cosmochim. Acta 61, 4429–4438.
Wickman, F.E., Åberg, G., Levi, B., 1983. Rb–Sr dating of alteration events in granitoids. Contrib. Mineral. Petrol. 83, 358–362.
York, D., Farquhar, R.M., 2013. The Earth's Age and Geochronology. Elsevier.